Computational Materials Science 2014, 84(327-338)

Microstructure evolution during dynamic discontinuous recrystallization in particle-containing Cu

Håkan Hallberg*†, Bob Svendsen‡, Tobias Kayser‡, Matti Ristinmaa†
†Division of Solid Mechanics, Lund University, Box 118, S-221 00 Lund, Sweden
‡Material Mechanics, RWTH Aachen University, D-52062 Aachen, Germany

Abstract

Control of the grain size in a material is vital in many engineering applications. Evolving through recrystallization, the grain size is strongly influenced by the presence of impurity particles. These particles exert drag forces on migrating grain boundaries and prevent grain boundary motion by pinning of the boundaries. Taking copper as example material, the present work establishes a novel simulation model where dynamic discontinuous recrystallization is influenced by particle drag. The recrystallization kinetics are established on a microlevel and the simulations are performed using a 3D cellular automaton algorithm with probabilistic cell state switches. By this approach, computational efficiency is combined with high temporal and spatial resolution of the microstructure evolution. The simulated microstructure changes are in good agreement with experimental findings and the recrystallization kinetics are shown to comply with classical Kolmogorov/Johnson/Mehl/Avrami (KJMA) theory. In addition, through homogenization, the macroscopic flow stress behavior is studied and is also shown to exhibit the expected transition from single-peak stable flow into serrated multiple-peak flow as the processing temperature is increased. Influence of changed initial grain sizes is studied and, in compliance with experimental data, an increased initial grain size stabilizes the flow stress behavior whereas the opposite trend is found for reduced initial grain sizes. Introducing impurity particles in the simulations, the progression of recrystallization is retarded and optimum values of the particle dispersion level are identified at different temperatures, allowing minimization of the recrystallized grain size during thermomechanical processing of the material.

Keywords: Dynamic recrystallization, Cellular automata, Grain boundary migration, Copper, Grain growth, Impurities

1 Introduction

The grain size of metallic materials has become an increasingly important parameter since it influences not only important material properties such as ductility and strength but also fatigue and wear properties, electrical properties and resistance to chemical attack. Further, in product miniaturization related to MEMS and biomedical devices, a close control of the grain size is required as the size of the objects is scaled down to the microlevel.

*hakan.hallberg@solid.lth.se

DOI: 10.1016/j.commatsci.2013.12.021

Driven by a lowering of the Gibbs energy in the material, recrystallization acts as the main mechanism for transforming the grain microstructure in metallic materials. The recrystallization may occur as a relatively slow and temperature-driven static process or it may proceed, driven by deformation, through dynamic recrystallization. The latter can be either a continuous or a discontinuous process. Continuous recrystallization works by dislocation cell formation and growth of subgrains whereas discontinuous recrystallization proceeds by nucleation and subsequent growth of new grains at high-energy sites in the microstructure, predominantly along grain boundaries. Whether the dynamic recrystallization proceeds as a continuous or a discontinuous process is largely dictated by the level of stacking-fault energy in the material. In high stacking-fault materials, such as aluminum, dynamic recovery is rapid in favor of continuous dynamic recrystallization. In contrast, in low stacking-fault materials such as copper, dynamic recovery is less influential, making discontinuous dynamic recrystallization the dominant recrystallization mechanism.

Materials undergoing recrystallization are characterized by oscillatory flow stress behavior. The tendency for flow stress serrations increases as the processing temperature is increased or as the strain rate is decreased, changing the behavior from single-peak flow into multiple peak flow [1, 2, 3, 4]. This is often attributed to the competing processes of work hardening and softening caused by recrystallization. At lower temperatures or under higher strain rates, several cycles of recrystallization may occur in parallel, damping out the flow stress oscillations. In contrast, at higher temperatures and lower strain rates, each cycle of recrystallization is more or less allowed to finish before the next one sets in, resulting in oscillatory flow.

Recrystallization can to a large extent be controlled by a careful setting of processing parameters such as the temperature and the rate of deformation. In addition, the presence of impurities and second-phase particles strongly influences the appearance and evolution of the material microstructure during recrystallization. This latter influence is, however, twofold since particles on one hand may restrict grain boundary mobility through Zener pinning while, on the other hand, the recrystallization process may be facilitated by particle stimulated nucleation (PSN) at the inclusions. Such nucleation may then occur also within the grain interiors and not exclusively along grain boundaries. This puts the need for solid understanding of the influence of impurities in the material during processing and also for the availability of proper simulation tools.

A theoretical treatment of recrystallization influenced by both Zener pinning and PSN is given in [4, 5, 6]. Recrystallization processes have also been studied through simulation previously using e.g. continuum mechanical models, Monte Carlo Potts, cellular automata algorithms and phase field models. Especially Monte Carlo Potts models have been frequently employed in recrystallization studies since the pioneering work in [7, 8, 9, 10] and also in [11].

The present paper contributes by formulating a cellular automaton model of dynamic discontinuous recrystallization (DDRX) in copper, also considering Zener pinning. To the author's knowledge, such 3D simulations of thermomechanical processing has not been previously studied in the literature.

Cellular automata have become increasingly used in computational materials science. Applications vary from studies of phase transformation, recrystallization and solid state precipitation to growth of spherulites in polymers and dendrite growth during solidification of melts [12, 13]. Cellular automata as a tool for recrystallization modeling was introduced in [14] and cellular automata models of DDRX are established in [15, 16, 17, 18]. Cellular automaton simulation of static recrystallization considering Zener pinning is presented in [19] and PSN is considered in [20]. In the present paper, a 3D cellular automaton model with probabilistic cell state switching rules is used. This provides excellent computational efficiency combined with high spatial and temporal

resolution of the microstructure evolution. Use of probabilistic cell state switches was introduced in [21, 22] and allows a physically justified representation of grain boundary kinetics in a cellular automaton setting, e.g. in terms of a physical time scale. The probabilistic cellular automaton is more related to Monte Carlo Potts models than purely deterministic cellular automata. However, the central concept of the Q-state Potts model, which is a generalization of the two-state Ising model, is energy minimization based on a random sampling of a fixed number of lattice site states. In a probabilistic cellular automaton, the probability is introduced to scale interface velocities based on locally computed quantities.

In the present model, DDRX occurs by nucleation of new grains at sites of sufficient dislocation density along the grain boundaries. Grain growth proceeds under the competing processes of stored energy reduction, grain boundary energy minimization and particle drag. PSN is not included presently since the two events of particle drag and particle stimulated nucleation occur at different ranges of particle sizes. In the present work, dispersions of relatively small ($<< 1$ μm) particles are considered. It can be noted, however, that it is straightforward to incorporate effects of particle stimulated nucleation in the present modeling framework. In the proposed model, a cellular automaton model resolving the grain microstructure is employed. With this spatial resolution, subgrains are not explicitly modeled, nor are the particles which are only present in a statistical sense. Nucleation of recrystallized grains is also assumed be unaffected by particles in the model. Formulating the model in this way means that particle/subgrain interaction is not treated and the effect of particles will be limited to retardation of grain boundary velocity and influence on the final recrystallized grain size. Studying the influence of particle size and particle volume fraction on the recrystallized grain size is a main focus of the present work.

The paper begins by establishing the recrystallization kinematics on a microlevel together with the evolution laws for dislocation density and grain embryo nucleation. The subsequent section describes the cellular automaton formulation after which model calibration and simulations of axisymmetric compression at elevated temperatures are shown. The microstructure evolution under different thermal conditions, and using different initial grain sizes, are studied. This is followed by a section on the influence of particles on the recrystallization kinetics. A discussion on the results follows and some concluding remarks closes the paper.

2 Recrystallization kinetics and evolution laws

When a metallic material is deformed through plastic slip, stored energy build-up will occur in terms of an increased dislocation density. If recovery by dislocation annihilation is slow as in materials of low stacking-fault energy, grain nuclei may start to form. The nucleation predominantly occurs along grain boundaries where enough stored energy is present [4, 23, 24]. In combination with recovery, the microstructure may reach a thermodynamically more favorable state by growth of new and relatively dislocation-free grains from the nuclei. Following the formulation in [25], the dislocation density ρ in a single grain is assumed to evolve according to a Kocks-Mecking relation on the form

$$\dot{\rho} = (k_1\sqrt{\rho} - k_2\rho)\,\dot{\varepsilon}^{\mathrm{p}}_{\mathrm{eff}} \tag{1}$$

where $k_{1,2}$ are parameters and $\dot{\varepsilon}^{\mathrm{p}}_{\mathrm{eff}}$ is the rate of the effective plastic strain. Note that a superposed dot denotes differentiation with respect to time.

The parameter k_1 is expected to be a constant while k_2 is generally found to be a function of temperature and strain rate. As discussed in [26], the parameters $k_{1,2}$ in eq. (1) can be estimated

from observations of the macroscopic flow stress behavior. If the second-stage hardening rate and the saturation flow stress is denoted by θ_{II} and σ_{s}, respectively, the Kocks-Mecking model results in

$$k_1 = \frac{2}{\alpha b}\frac{\theta_{\mathrm{II}}}{\mu} \qquad \text{and} \qquad k_2 = \alpha\mu b\frac{k_1}{\sigma_{\mathrm{s}}} \tag{2}$$

where μ is the shear modulus, b the magnitude of the Burgers vector and α a numerical constant. By eq. (2a), the k_1-parameter will exhibit small variations with temperature due to the presence of the temperature dependent shear modulus μ. One possibility to achieve a constant value of k_1 would be to take the mean value. However, since k_1 varies only slightly, or is "virtually constant" as noted in [27], eq. (2a) is presently accepted as an estimate for the parameter k_1. This is further discussed in Section 3, where material parameters for pure Cu are established and a nearly constant value of k_1 is found.

The hardening rate θ_{II} can be directly obtained from macroscopic flow stress data and following e.g. [28], the saturation stress σ_s can also be determined from experimental data by observing the proportionality

$$\log\left(\frac{\sigma_{\mathrm{s}}}{\mu}\right) \propto g\left(T, \dot{\varepsilon}^{\mathrm{p}}_{\mathrm{eff}}\right) \tag{3}$$

where the function g is given by

$$g\left(T, \dot{\varepsilon}^{\mathrm{p}}_{\mathrm{eff}}\right) = \frac{k_{\mathrm{B}}T}{\mu b^3}\ln\left(\frac{\dot{\varepsilon}_{\mathrm{ref}}}{\dot{\varepsilon}^{\mathrm{p}}_{\mathrm{eff}}}\right) \tag{4}$$

Here, k_{B} is the Boltzmann constant, T the absolute temperature and $\dot{\varepsilon}_{\mathrm{ref}}$ a reference strain rate.

If impurities such as second-phase particles are present in the material they will to some extent influence the evolution of dislocation density by a reduction of the rate of dynamic recovery. As suggested in [29, 30], this influence could be incorporated into eq. (1) by a scaling of the k_2 parameter, depending on the influence of particles. This is, however, not pursued further in the present model.

The present model considers a constant value of the dislocation density within each grain. This is a simplifying approach to the inhomogeneous distribution of dislocation density that is to be expected due to the influence of grain boundaries. Since grain boundaries pose obstacles to dislocation migration, accumulation of dislocations will occur in the vicinity of the grain boundaries. One method of incorporating this kind of grain boundary-dependent dislocation accumulation in CA models is introduced in [31]. The approach taken in [31] is based on treating the evolution of the dislocation density as a reaction-diffusion system with a distinction between mobile and immobile dislocations in conjunction with the immobilization of dislocations occurring at the grain boundaries.

If the particles are of such size (> 1 μm) that enough lattice curvature is created in their surrounding, new grains may appear due to particle stimulated nucleation (PSN) in the grain interiors. However, the present study concerns dispersions of finer particles ($<< 1$ μm), making grain boundary nucleation the absolutely dominant nucleation mechanism. PSN is hence not considered here, although it certainly possible to incorporate it in the present modeling framework.

Nucleation of new grains during dynamic discontinuous recrystallization is commonly accepted to occur due to instabilities in dislocation structures. Under favorable conditions, individual subgrains may grow to form recrystallization nuclei. Classically, mesoscale models of dynamic recrystallization treat the nucleation event by assuming either site-saturated nucleation – where

all nuclei are present from the start of the simulation – or continuous nucleation – where nuclei are continuously provided at a constant rate [4]. For computational efficiency, subgrain dislocation structures are not resolved in the present model and as a simplifying assumption, nucleation is described by a constant rate of nucleation which, per unit of grain boundary area, is taken as

$$\dot{n} = c(T)\dot{\varepsilon}^{\mathrm{p}}_{\mathrm{eff}} \exp\left(-\frac{Q_{\mathrm{n}}}{RT}\right) \tag{5}$$

where T is the absolute temperature, $c(T)$ is a temperature dependent parameter, R the gas constant and Q_{n} the activation energy for nucleation. This corresponds to the proportional nucleation model of [32, 33] which has also been used by e.g. [34, 16, 35]. It should be noted, however, that the extent of the nucleation is influenced by $c(T)$ that decreases with increasing temperature. This yields a temperature dependence of the nucleation rate that is in agreement with what is suggested in [36]. The influence of $c(T)$ is discussed further later on, as parameter values for pure copper are introduced.

The nucleation activation energy in (5) is for simplicity taken as a constant parameter in the present model whereas this quantity is likely to depend on the state of the microstructure at a given location, e.g., in terms of the energy stored locally. It can also be noted that the rate of nucleation in eq. (5) for simplicity is assumed to be unaffected by the presence of particles although nucleation is likely to be inhibited by particles stabilizing the subgrain structure.

As discussed previously, nucleation predominantly occur along grain boundaries at sites where sufficient stored energy is present. Following [37], this process is viewed as a bulging of the grain boundary, locally initiated once a critical dislocation density ρ_{c} is reached, also cf. [38]. The critical dislocation density ρ_{c} thus serves as a threshold value for nucleation during the recrystallization process. The critical dislocation density is further considered in relation to calibration of the model. It can be noted that the critical dislocation density employed in the present work corresponds to the often used concept of a macroscopic critical strain and a corresponding macroscopic critical stress at initiation of recrystallization.

The grain boundary migration velocity is directed along the local grain boundary normal and the velocity magnitude is given by

$$v = mp \tag{6}$$

where m is the grain boundary mobility and p the pressure available to drive the grain boundary motion. Such recrystallization and grain growth kinetics were addressed already in [39] where the migration of grain boundaries under the influence of a driving force was studied. The grain boundary mobility m is in the present model assumed to be a function of the absolute temperature and the relative grain misorientation. The mobility is by this approach allowed to vary throughout the microstructure under consideration.

Following the derivation presented in [25], the driving pressure p can – in the absence of Zener drag – be viewed to consist of two terms p_{D} and p_{C}, related to the jump in dislocation density across the boundary $[\rho]$ and to the grain boundary energy γ, respectively. These terms appear as

$$\begin{aligned} p_{\mathrm{D}} &= \tau[\rho] \\ p_{\mathrm{C}} &= -\frac{2\gamma}{r} \end{aligned} \tag{7}$$

rendering a driving pressure on the form $p = p_{\mathrm{D}} + p_{\mathrm{C}}$. In eq. (7a), the dislocation line energy is defined as $\tau = \mu b^2/2$ where μ is the shear modulus. The local grain boundary curvature $1/r$

enters the formulation in (7b) and will be discussed later on in relation to establishing the cellular automaton algorithm.

Impurity atoms not properly fitted in the material microstructure will segregate to the grain boundaries to achieve better accommodation. The accumulation of impurity atoms will lead to a lowering of the grain boundary energy, making it increasingly difficult for the boundary to migrate away from the segregated atoms. Interstitial atoms such as oxygen may cause this pinning effect, cf. [40]. While high-purity materials can undergo recrystallization at relatively low temperatures, recrystallization in a lower-purity material may have to be facilitated by raised process temperatures. The pinning pressure exerted on the boundary due to second-phase particles may be generally expressed as

$$p_{\mathrm{Z}} = -z_1 \gamma_0 \frac{f_{\mathrm{v}}^{z_2}}{r_{\mathrm{p}}} \tag{8}$$

where z_i are constants and where f_{v} is the volume fraction of particles with radius r_{p}. The interface energy γ_0 enters eq. (8) as a constant parameter since it is not related to the misorientation energy between particle and matrix material, but is directly related to the local interface energy that is proportional to the interface curvature. In contrast, the grain boundary energy γ in eq. (7b) will be allowed to vary with the relative grain misorientation, as is shown later on. In eq. (8), the interface energy is related to the boundary between the particle inclusion and the surrounding bulk material. The drag force p_{Z} in eq. (8) may be substantial if the size of the dispersed particles is small (diameter < 1 μm). The original formulation by Zener [41], perhaps best denoted the "Smith-Zener formulation" and given by $z_i = [3/2, 1]$, is established under the assumption of rigid grain boundaries. Different remedies to account for the tendency for the grain boundary to bow out between pinning particles have been proposed. Such a modified formulation of the Zener drag pressure, where the influence of the volume fraction of solute atoms is emphasized, was put forward in [42, 43, 44] and is obtained by setting $z_i = [0.33, 0.87]$, valid for values of f_{v} below 3%. In [45], $z_2 = 1$ was arrived at. Including the Zener drag in the expression for the boundary driving pressure renders the format

$$p = p_{\mathrm{D}} + p_{\mathrm{C}} + p_{\mathrm{Z}} \tag{9}$$

The grain boundary energy, γ, first appearing in eq. (7b), is related to the relative misorientation θ between adjacent grains. As a more general alternative to the Read-Shockley formulation for the grain boundary energy, which is limited to small misorientation values, we adopt the modified formulation in [46, 25] which appears as

$$\gamma = \gamma_0 \sin(2\theta) \left\{1 - r_\gamma \ln\left[\sin(2\theta)\right]\right\}, \quad 0 \leq \theta \leq 90^\circ \tag{10}$$

where r_γ is a constant, specified below along with the interface energy γ_0 in relation to calibration of the model against experimental data. According to [46], the grain boundary energy variation with misorientation, as described by eq. (10), is in good agreement with grain boundary energy simulation results for symmetric twist and tilt boundaries in the misorientation range $0 \leq \theta \leq 90^\circ$.

The orientation of the grains in the microstructure is in the present model described using the Bunge-Euler angles $\{\varphi_1, \Phi, \varphi_2\}$. From these angles a corresponding orientation matrix $\boldsymbol{R}(\varphi_1, \Phi, \varphi_2)$ may be constructed [47]. Letting $\boldsymbol{R}_1$ and $\boldsymbol{R}_2$ denote the orientations of two adjacent grains, the orientation difference between them is obtained as $\Delta\boldsymbol{R} = \boldsymbol{R}_2 \boldsymbol{R}_1^{\mathrm{T}}$ where $(\cdot)^{\mathrm{T}}$ denotes the transpose. In order to obtain a single scalar measure of the misorientation we follow the approach

in [48, 49, 50] whereby the orientation difference between the two neighboring grains is written as

$$\theta = \arccos\left[\frac{\mathrm{tr}\left(\Delta \boldsymbol{R}\right) - 1}{2}\right] \tag{11}$$

where $\mathrm{tr}(\cdot)$ denotes the trace of a matrix. Eq. (11) does not explicitly consider crystallographic symmetry, but is employed in the present work for simplicity and for computational efficiency.

Turning next to the mobility m of the grain boundaries, the mobility is taken to depend on both temperature and relative misorientation between the two adjacent grains. Following [4, 35, 51], the mobility is taken as

$$m\left(T, \theta\right) = \widetilde{m}_0\left(T, \theta\right) \exp\left(-\frac{Q_\mathrm{m}}{RT}\right) \tag{12}$$

where Q_m is the activation energy for boundary migration. As suggested in [5], the pre-exponential term $\widetilde{m}_0$ is made dependent on the grain misorientation according to

$$\widetilde{m}_0\left(T, \theta\right) = m_0\left(T\right)\left(1 - \exp\left[-B\left(\frac{\theta}{\theta_\mathrm{m}}\right)^k\right]\right) \tag{13}$$

where $\theta_\mathrm{m} \approx 15^\circ$ is the misorientation angle, differentiating between low- and high-angle boundaries and where B and k are parameters, further considered during the calibration of the model later on. The quantity m_0 corresponds to the mobility of high-angle grain boundaries and is proportional to the inverse of the absolute temperature [4], i.e.

$$m_0\left(T\right) \propto \frac{1}{T} \tag{14}$$

The recrystallization process may now be described by nucleation according to (5) and subsequent growth by (6), with driving pressure and boundary mobility given by (9) and (12).

3 Cellular automaton formulation

A 2D cellular automaton model for simulation of discontinuous dynamic recrystallization in copper was established in the preceding paper [25]. That model is here reformulated according to the previous section and is also extended to 3D using Moore neighborhoods and cubic cells. A representative volume element (RVE) is constructed as a cube with side length 256 μm. The volume is discretized using 256^3 cubic cells, each with a side length of 1 μm. An initial grain structure is generated by letting a certain number of randomly placed nuclei grow until they impinge upon each other, cf. Fig. 1. The morphology of the initial microstructure will resemble a Voronoi construction rather than a physical sample but the simulation is assumed to be relatively unaffected by this approach. With the size of the RVE fixed, the chosen number of nuclei will dictate the average grain size of the initial microstructure. Each grain is then given a random initial dislocation density from a normal distribution with mean 10^{11} m^{-2} and standard deviation 10^{10} m^{-2}, representative for the annealed state [52]. For simplicity, the dislocation density is assumed to be homogeneously distributed within each grain. The grains, constituting the initial microstructure, are also given random orientations from a uniform distribution, rendering an initially isotropic orientation distribution. The initial material to be in an annealed and undeformed state according to the description in [53]. This suggest the assumption of a random initial texture made in the present work. Let ξ_i denote three random numbers from this distribution in the interval $[0, 1]$.

Figure 1: Initial grain structure of the cellular automaton representative volume element with dimensions $256 \times 256 \times 256$ μm. The colors are randomly applied to distinguish between grains.

Following [47, 54], the initial orientations are then obtained from

$$\begin{aligned} \varphi_1 &= 2\pi\xi_1 \\ \Phi &= \arccos\left(1 - 2\xi_2\right) \\ \varphi_2 &= 2\pi\xi_3 \end{aligned} \tag{15}$$

Each cell is assigned state variables, which in the present case consist of the dislocation density, the three Bunge-Euler angles, an indicator specifying if the cell is recrystallized or not and also an identifier, stating to which grain the cell belongs. The state of the cells in the cellular automaton is determined either by evolution laws – e.g. for the dislocation density, cf. eq. (1) – or by some switching rule which can be deterministic or probabilistic. The latter is considered when determining to which grain a cell belongs since the grain boundary migration velocities will vary throughout the analysis domain. To avoid the nonphysical situation where all grain boundaries are allowed to migrate one cell distance during a common time step, a probabilistic cell state switch is employed as in [25]. The maximum local grain boundary velocity in the analysis domain is denoted by $v_{\max}$ which allows definition of the ratio

$$w_{\text{growth}} = \frac{v}{v_{\max}} \quad \text{where} \quad v \leq v_{\max} \tag{16}$$

Next, when a cell is approached by a moving grain boundary with velocity v, a random number $\xi \in [0, 1]$ is generated. If $\xi \leq w_{\text{growth}}$, the cell is consumed by the approaching grain, otherwise it is not. Due to the formulation in eq. (16), a cell in front of the grain boundary moving at the local velocity $v_{\max}$ will have a switching probability of 1.

A similar probabilistic switching rule is used during the nucleation of new grain embryos, cf. [25]. The number of new nuclei to appear is determined by eq. (5). All possible nucleation sites with a dislocation density greater than ρ_{c} are considered and the highest dislocation density is

denoted by $\rho_{\max}$. A dislocation density ratio is defined according to

$$w_{\text{nucl}} = \frac{\rho}{\rho_{\max}} \quad \text{where} \quad \rho_{\text{c}} \leq \rho \leq \rho_{\max} \tag{17}$$

Again a random number $\xi \in [0, 1]$ is generated and the current location is accepted as a viable nucleation site if $\xi \leq w_{\text{nucl}}$. By this approach, the site with the highest dislocation density, $\rho_{\max}$, will have a nucleation probability of 1. The sites are checked until all nuclei to appear during the time step are placed. Consumption of the most dislocation dense sites is also consistent with the recrystallization striving to efficiently lower the stored energy in the material.

For calculation of the local grain boundary radius r, an extended cell neighborhood is used, including the first-, second and third-nearest cell neighbors. The radius is obtained by evaluating

$$r = a_{\text{r}} \frac{n+1}{n_k - n_i} \tag{18}$$

where a_{r} is a parameter discussed further later on, n is the total number of neighbor cells, n_i is the number of neighbors within the current neighborhood that belongs to the grain and n_k is the number of neighbor cells belonging to an adjacent grain if it approaches the current cell with a locally planar boundary for which $n_k = n_i$ and $r \to \infty$ is obtained. This approximation for the local boundary curvature has been used previously in [55, 56, 25]. In the present case, $n = 342$ and $n_k = 147$ are used.

Since the cell grid of the cellular automaton implies a fixed spatial resolution, the cell size puts an upper limit to the allowable growth distance for a grain boundary in a single time step. The grain growth kinetics in the algorithm have to be tuned in accord with the chosen spatial resolution. This can be achieved by considering eqs. (6) and (9). For a given difference in dislocation density $[\rho]$ and for a given misorientation θ, these equations provide an analytic expression for the grain boundary velocity, and hence also for the grain boundary radius. Considering a cellular automaton-formulated RVE with a single grain embedded in a homogeneous matrix, the grain growth kinetics can be tuned. To this end, let λ_{c} denote the growth distance traveled by a migrating grain boundary with the reference boundary velocity v_{c} during a time increment Δt_{c}, i.e. $\lambda_{\text{c}} = v_{\text{c}} \Delta t_{\text{c}}$. A one-grain simulation is then performed by setting $[\rho] = 1 \times 10^{15}$ and $\theta = 45°$. Remaining parameters are set as $k_1 = 379.5$ m^{-1}, $k_2 = 1.3 \times 10^{-5}$, $M_0 = 0.65 \times 10^{-5}$ m·s^{-1}, $\rho_{\text{c}} = 9.10 \times 10^{14}$ m^{-2}, $\mu = 30$ GPa, $b = 0.256$ nm, $\gamma_0 = 0.625$ J·m^{-2} and $r_\gamma = 0.66$. These values correspond to the behavior of pure copper at a temperature of 725 K. The result of the one-grain simulation is shown in Fig. 2 and was obtained by choosing $\Delta t_{\text{c}} = 0.12$ s, $v_{\text{c}} = 3$ μm/s and $a_{\text{r}} = 0.45$ μm. Note that in Fig. 2, the label "Calculated radius" refers to the grain radius integrated directly using the velocity $v = mp$ in eq. (6) with $p = p_{\text{D}} + p_{\text{C}}$ according to eq. (8) together with the time incrementation of a cellular automaton run. The label "Grid-based radius" in Fig. 2 refers to the radius obtained from a grain growing in the cellular automaton cell grid during the same simulation. The radii shown in Fig. 2 are thus obtained using a non-constant growth velocity. In a poly-crystal simulation, the time step Δt in the cellular automaton can now be obtained by a scaling of the maximum current grain boundary velocity $v_{\max}$ according to $\Delta t = \lambda_{\text{c}} / v_{\max}$.

Next, considering a polycrystalline RVE, it is noted that the strain rate independent macroscopic flow stress according to e.g. [26] relates to the average dislocation density $\bar{\rho}$ according to

$$\hat{\sigma} = \alpha \mu b \sqrt{\bar{\rho}} \tag{19}$$

where α is a parameter related to the dislocation interaction strength [62].

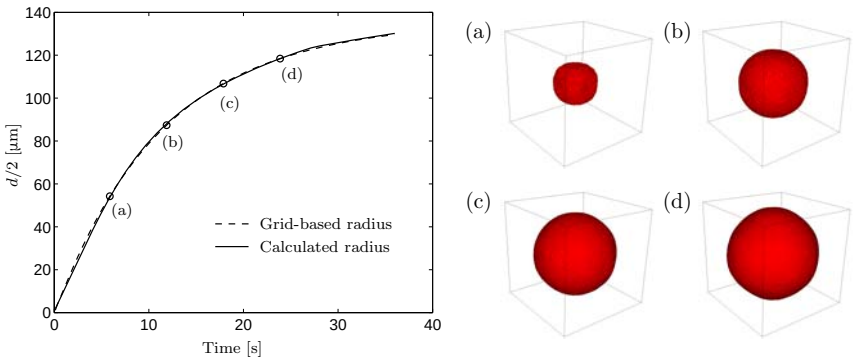

Figure 2: Growth rate of a grain obtained by direct calculation (solid line) and obtained using a cellular automaton simulation (dashed line). The cellular automaton grain is shown at four different growth stages in pictures (a)-(d) to the right.

Table 1: Material parameters entering the present model. The values pertain to copper.

Parameter	Value	Description	Used in eq.	Source
T_m	1356 K	Melting temperature	(20)	[57]
θ_II	1.1×10^9 Pa	Second-stage hardening rate	(2)	[36]
$\dot{\varepsilon}^\mathrm{p}_\mathrm{ref}$	1×10^7 s^{-1}	Reference strain rate	(4)	[28]
$\dot{\varepsilon}^\mathrm{p}_0$	4.5×10^{-7} s^{-1}	Reference strain rate	(23)	[58]
m	0.0222	Strain rate sensitivity exponent	(23)	[58]
γ_0	0.625 J·m^{-2}	Grain boundary energy	(10)	[4]
r_γ	0.66	Grain boundary energy parameter	(10)	[59]
α	0.35	Dislocation interaction strength parameter	(2), (19)	[36]
Q_m	126 kJ·mol^{-1}	Activation energy for grain boundary migration	(12)	[60]
θ_m	15°	Angle at shift from LAGB to HAGB	(13)	[4]
b	0.256 nm	Magnitude of the Burgers vector	(2), (4), (19)	[61]
Q_n	261 kJ·mol^{-1}	Activation energy for nucleation	(5)	[53]
B	5	Parameter in the mobility misorientation dependence	(13)	[5]
k	4	Parameter in the mobility misorientation dependence	(13)	[5]

The temperature dependence of the shear modulus is, following [63], taken as

$$\mu\left(T\right) = 35.4 \times 10^9 \left[1 - 0.5\left(\frac{T - 300}{T_{\mathrm{m}}}\right)\right] \quad \mathrm{Pa} \tag{20}$$

where $T_{\mathrm{m}} = 1356$ K is the melting temperature for pure copper. The average dislocation density is obtained by considering a homogenization of the plastic work power, denoted by $\dot{w}^{\mathrm{p}}$, i.e.

$$\dot{w}^{\mathrm{p}} = \hat{\sigma}\dot{\varepsilon}^{\mathrm{p}}_{\mathrm{eff}} = \frac{1}{V}\sum_i \int_{V_i} \dot{w}^{\mathrm{p}}_i dV = \frac{1}{V}\sum_i \int_{V_i} \hat{\sigma}_i \dot{\varepsilon}^{\mathrm{p}}_{\mathrm{eff},i} dV \tag{21}$$

Here a subscript i indicates quantities related to grain i and the total volume of the RVE is denoted by V. Using $\hat{\sigma}_i = \alpha\mu b\sqrt{\rho_i}$ and $\dot{\varepsilon}^{\mathrm{p}}_{\mathrm{eff}} = \dot{\varepsilon}^{\mathrm{p}}_{\mathrm{eff},i}$ results in

$$\sqrt{\overline{\rho}} = \frac{1}{V}\sum_i \int_{V_i} \sqrt{\rho_i} dV \tag{22}$$

Note that in eqs. (21) and (22), the summations are performed over all grains.

For simplicity, a Taylor assumption is employed in the present homogenization scheme, whereby $\dot{\varepsilon}^{\mathrm{p}}_{\mathrm{eff}} = \dot{\varepsilon}^{\mathrm{p}}_{\mathrm{eff},i}$ is assumed as the elastic strains are negligible. It can be noted that alternative formulations exist, such as the iso-work assumption suggested in [64]. A more rigorous homogenization procedure would be to consider a multilevel formulation, where the macroscopic deformation is enforced as a periodic boundary condition on the microlevel RVE. However, the Taylor assumption is frequently employed in crystal plasticity models of polycrystal plasticity and was also used in a mean field model of dynamic discontinuous recrystallization in [51].

Following e.g. [26], the dependence of the macroscopic flow stress on strain rate is introduced by considering eq. (19) and formulating

$$\sigma = \hat{\sigma}\left(\frac{\dot{\varepsilon}^{\mathrm{p}}_{\mathrm{eff}}}{\dot{\varepsilon}_0}\right)^m \tag{23}$$

where m is a strain rate sensitivity parameter and $\dot{\varepsilon}_0$ a reference strain rate, different from $\dot{\varepsilon}_{\mathrm{ref}}$ in eq. (4)

For the saturation stress, σ_{s}, eqs. (3) and (4) are fitted to experimental data on pure copper in [36], giving

$$\log\left(\frac{\sigma_{\mathrm{s}}}{\mu}\right) = -2.271g - 1.654. \tag{24}$$

In addition, the second-stage hardening rate is in [36] determined as $\theta_{\mathrm{II}} = 1.1 \times 10^9$ Pa. It can be noted that in [36], the values of σ_{s} and θ_{II} are based on experimental data from a limited temperature interval and the precision at very high temperatures must be treated with some caution.

Material parameters for pure copper are summarized in Table 1.

From eq. (2a) the parameter k_1, related to the athermal accumulation of dislocations, can be estimated from the relation $k_1 = 2\left(\theta_{\mathrm{II}}/\mu\right)\left(\alpha b\right)^{-1}$, cf. [26]. Due to the shear modulus μ being temperature dependent according to eq. (20), a slight variation in the ratio θ_{II}/μ is observed as the temperature is varied. However, following [27], eq. (2a) is accepted as an estimate of the k_1-parameter as the variations are small. Choosing values of θ_{II}, b and α according to Table 1 and with μ calculated from eq. (20), the value of k_1 will vary from 5.8×10^8 m^{-1} at $T = 725$ K to 6.8×10^8 m^{-1} at $T = 1075$ K. As noted previously, the experimental data at $T = 1075$ K should

Table 2: Temperature dependencies of the critical dislocation density ρ_c, the nucleation parameter c and the mobility parameter m_0.

T [K]	ρ_c [m^{-2}]	m_0 [$m \cdot s^{-1}$]	c [m^{-3}]
725	5.70×10^{14}	1.32×10^{-5}	6×10^{24}
775	3.70×10^{14}	1.1×10^{-5}	4×10^{23}
875	1.46×10^{14}	0.72×10^{-5}	7×10^{20}
975	5.30×10^{13}	0.32×10^{-5}	3×10^{19}
1075	1.72×10^{13}	0.23×10^{-5}	7×10^{17}

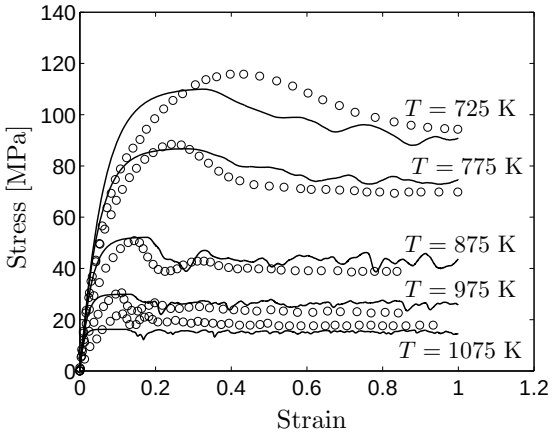

Figure 3: Flow stress behavior at five different temperatures. Experimental results, taken from [53] are shown by circles and simulation results from the present work are shown by solid lines. In both simulations and experiments, the initial grain size was $d_0 = 78$ μm.

be read with some caution. For the reduced temperature range $725 - 975$ K, the value of the k_1-parameter varies between 5.8×10^8 m^{-1} and 6.5×10^8 m^{-1}.

By setting the temperature dependent parameters related to the critical dislocation density for nucleation, boundary mobility and rate of nucleation according to Table 2, the macroscopic flow stress behavior in Fig. 3 is obtained. The effective plastic strain rate is in the simulations kept constant at $\dot{\varepsilon}_{\text{eff}} = 2 \times 10^{-3}$ s^{-1}. Regarding the mobility parameter m_0 in Table 2, it can be noted that this quantity decreases with increasing temperature, in agreement with eq. (14). Also, the decreasing values of the nucleation parameter c with increasing temperature can be noted. This temperature dependence gives a nucleation rate that corresponds to the observations made in [36]. The simulation results in Fig. 3 are shown together with experimental data taken from [53]. In accordance with the experimental results, the simulated recrystallization proceeds more rapidly as the temperature is increased. This results in oscillatory flow stress behavior at higher temperatures, which is evident from Fig. 3. At lower temperatures, each recrystallization cycle is allowed to finish before the next one sets in, resulting in a more stable flow stress behavior. In contrast, at higher temperatures, new cycles of recrystallization are initiated before the preceding have completed. This causes the flow stress serrations seen in Fig. 3.

Nearly all aspects of the modeled material behavior are defined by the constants that are summarized in Table 1. However, in order to verify that the proposed model is able to capture the macroscopic flow stress behavior of pure Cu a separate set of experimental data, taken from [53], is also considered to provide the experimental flow stress curves in Fig. 3.

Having defined the material behavior by the constants in Table 1, only the three parameters ρ_{c}, m_0 and c are left to permit adjustment of the modeled material behavior to comply with the experimental flow stress data in [53]. These three parameters are taken as constants at a given temperature and are summarized in Table 2. The values of these parameters are found by fitting the macroscopic flow stress, obtained from the model, to the experimental flow stress data at each temperature. In addition, the three parameters are identified such that the final average grain size obtained in the simulations corresponds to the experimentally identified value at each temperature.

The modeled flow stress curves in Fig. 3 are found to be higher than the experimental values at some temperatures and lower at other. Part of the explanation for this is the identification of the three parameters in Table 2 but the main cause is the temperature dependence of the saturation flow stress σ_{s} in eqs. (3) and (4) that follows from the material constants in Table 1. Small differences in metal purity and variations in the experimental procedures cause some deviations between the experimental data in Table 1 and the experimental flow stress curves in Fig. 3, which are by purpose taken from a different source to allow some degree of verification of the model.

With the initial microstructure shown in Fig. 1, the grain structures obtained after simulated axisymmetric hot compression at different temperatures are shown in Fig. 4. These microstructures correspond to the flow stresses in Fig. 3. It can be noted that at the highest temperature of 1075 K, the microstructure evolution actually results in grain coarsening, as opposed to the grain refinement at lower temperatures. This observation is in line with the experimental data in [53]. Fig. 4 also shows the resulting average grain size d_{f}, obtained for a strain of $\varepsilon^{\text{p}}_{\text{eff}} = 1$ at each temperature. The saturation grain sizes obtained from the simulations are in good agreement with the grain sizes that were measured in [53], stated in Fig. 4 within parentheses.

Letting X denote the volume fraction of recrystallized material, the recrystallization kinetics are commonly described by Kolmogorov/Johnson/Mehl/Avrami (KJMA) theory by employing the

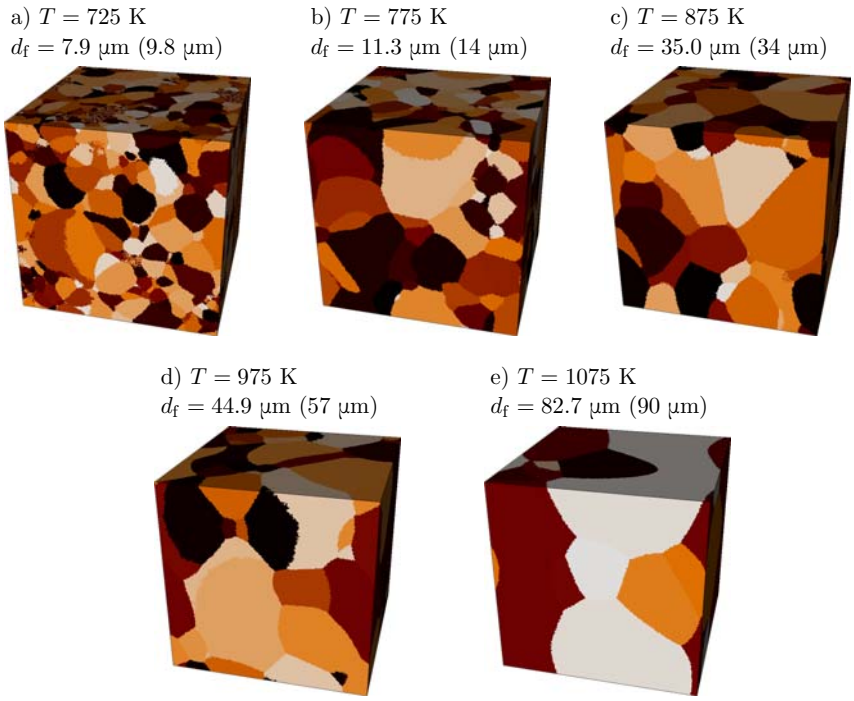

Figure 4: Resulting microstructure at 100 % strain at five different temperatures. In all cases, the initial grain size was $d_0 = 78$ μm. The final average grain sizes, obtained from the simulations, are denoted by d_f. The final grain size, observed in experiments according to [53], are stated within parentheses at each temperature.

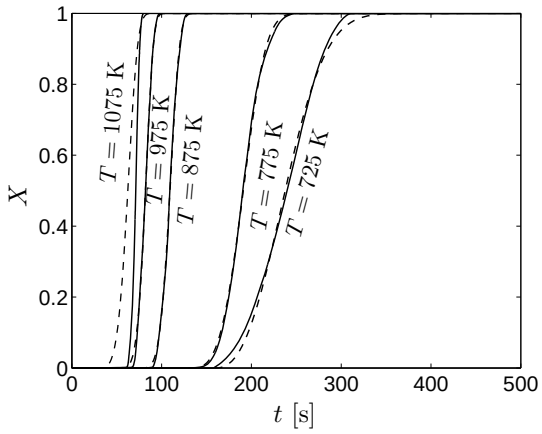

Figure 5: Recrystallization kinetics represented by the volume fraction of recrystallized material, denoted by X, as function of time, t, at five different temperatures. Solid lines show simulation results and dashed lines show the KJMA relation fitted to the simulation results at each temperature. Note that the plots at $T = 775$ K, $T = 875$ K and $T = 975$ K nearly coincide.

Table 3: Fitted KJMA parameters.

T [K]	n_{x}	B_{x}
725	2.5	1.1×10^{-5}
775	3.3	7.2×10^{-7}
875	4.5	7.6×10^{-8}
975	5.1	1.4×10^{-8}
1075	4.3	6.7×10^{-8}

relation

$$X = 1 - \exp\left(-B_{\mathrm{x}} t^{n_{\mathrm{x}}}\right) \tag{25}$$

where t is the time, B_{x} is a coefficient and n_{x} the Avrami exponent [65, 66, 67]. In Fig. 5a, the volume fraction of recrystallized material is plotted with solid lines. The KJMA equation (25), fitted by a least-squares procedure, is drawn with dashed lines at each temperature. The fitted KJMA parameters are shown in Table 3.

The KJMA model in eq. (25) was established under the assumption of site-saturated and homogeneous nucleation along with constant grain boundary velocities. As experimental results are considered, where both heterogeneous nucleation and non-constant migration velocities are encountered, deviations from the linear KJMA relation, cf. Fig 5b, inevitably occur. These deviations are accentuated during the initial stages of recrystallization where the assumption of site-saturated nucleation is least applicable and during the final stages where growing recrystallized grains to a large extent have consumed the possible nucleation sites in the microstructure. In the case of a constant nucleation rate, presently under consideration, experimental results indicate an Avrami exponent of $n_{\mathrm{x}} = 4$ to be expected whereas $n_{\mathrm{x}} = 3$ applies to site-saturated nucleation [4]. Considering the nucleation parameter c, cf. Table 2, it can be noted that going down in temperature the value of c increases, with the exception of the highest temperature $T = 1075$ K. A high value of c will result in all possible nucleation sites of the current microstructure being populated by nuclei, i.e. a situation of site-saturated nucleation. The reversed trend is encountered

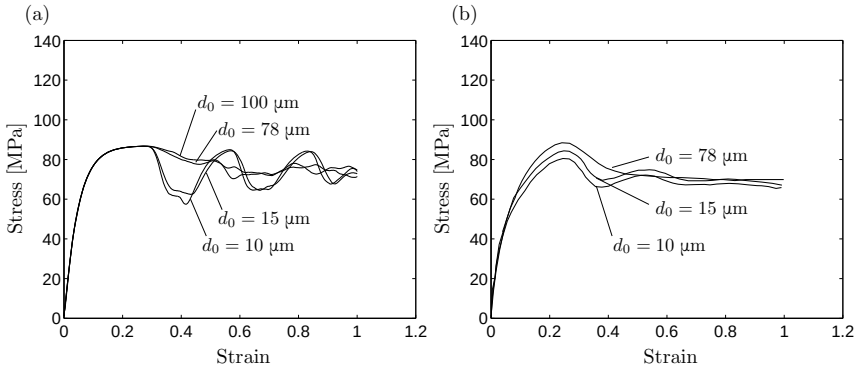

Figure 6: Influence of initial grain size on the flow stress behavior at $T = 775$ K. (a) Simulation results with four different initial grain sizes: $d_0 = 100$, 78, 15 and 10 μm. (b) Experimental results at the same temperature, taken from [53], showing the transition with decreasing initial grain size from single-peak flow at $d_0 = 78$ μm to oscillating flow at $d_0 = 15$ and 10 μm.

as the temperature is increased. This behavior is clearly shown in Fig. 5, where the slope of the KJMA function (dashed lines) changes from $n_{\mathrm{x}} \approx 2.5$ at $T = 725$ K to $n_{\mathrm{x}} \approx 5.1$ at $T = 975$ K, in qualitative agreement with KJMA theory.

As noted previously, the simulation results obtained at $T = 1075$ K should be interpreted cautiously. Values of the second-stage hardening rate θ_{II} and the saturation stress σ_{s} were defined in Section 3. As mentioned there, these parameter values were obtained from experimental data in a temperature interval not quite spanning the temperatures considered in Figs. 3 and 5. This is a probable cause for some of the deviations between the simulated macroscopic flow stress behavior and the experimental data in Fig. 3. In addition, following the study on dynamic recrystallization in copper single crystals in [68], it can be expected that the recrystallization behavior changes at a temperature of approximately $0.75T_{\mathrm{m}} \approx 1020$ K which results in a different nucleation behavior that at lower temperatures. This condition also separates the results at $T = 1075$ K in Figs. 3 and 5 from those obtained at lower temperatures.

It can also be noted that the original KJMA model has been reformulated and elaborated in numerous publications, e.g. [69, 70], but for simplicity the original formulation is employed in the present study.

The initial average grain size will influence the flow stress characteristics during recrystallization. This is shown in Fig. 6 at $T = 775$ K. Fig. 6a shows the simulated flow stress behavior and Fig. 6b experimental results from [53]. If the initial grain size is decreased, the volume fraction of grain boundaries, and hence the number of possible nucleation sites in the microstructure, increases. This permits repeated and simultaneous cycles of recrystallization to take place, resulting in an oscillatory flow stress behavior. In contrast, if larger initial grain sizes are considered, the number of possible nucleation sites are reduced which slows down the recrystallization process and stabilizes the flow stress behavior.

3.1 Parallel implementation of the cellular automata algorithm

One of the benefits of working with cellular automaton algorithms is their suitability for computer parallelization. Since the state of each cellular automaton cell is based solely on the previous state of the cell and the states of the nearest cell neighbors, information between cells only have to be communicated locally. This allows the updating scheme for the computational domain to be split

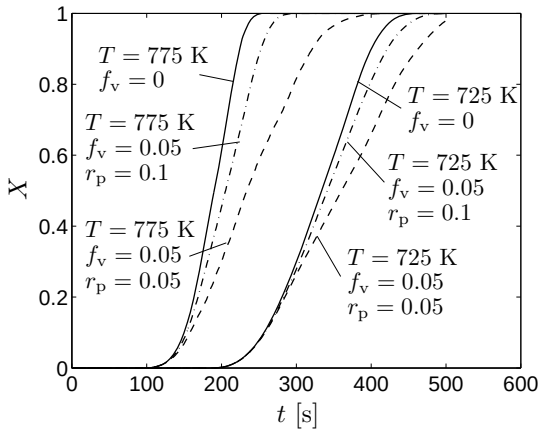

Figure 7: Influence on recrystallization from a homogeneous distribution of small impurity particles at $T = 725$ K and $T = 775$ K. The particles are of radius r_p (in μm) and are present by a volume fraction f_v. The rate of recrystallization is seen to decrease due to Zener pinning and more so for smaller particles.

into parallel processes.

In the present model, the domain is discretized into $256^3 \approx 16,800,000$ cells and for simplicity an OpenMP parallelization is employed. Using OpenMP, the parallel processors need to be connected to a shared memory in contrast to parallelization by using message passing interfaces, MPI. The latter approach would allow splitting of the computational effort between arbitrary numbers of processors while OpenMP limits the parallel execution to be performed on a single computer or cluster node.

Using four processor cores on a standard desktop computer, the present OpenMP implementation results in execution times of approximately six to eight hours for performing a full simulation run at a single temperature. The four cores reside on a processor of type "Intel Xeon W3520", working at 2.67 GHz.

Despite the large number of cells, which provides a substantial spatial resolution in the model, the required execution time is thus limited. In addition, the benefit of parallel execution increases with the number of processors being employed, allowing the computational time to be further reduced if additional processors were to be used. Even more speed-up could be expected if MPI parallelization would be employed with a larger number of parallel processors.

4 Influence of impurity particles

So far a pure copper material has been considered. In practical applications, however, a certain volume fraction of impurities is present in the material. These particles may indeed be impurities but can also be particles deliberately added in order to exert control over the grain size in the material during thermomechanical processing. Such tailoring of the material microstructure is becoming increasingly important in many industrial processes and for a wide range of metals and alloys including structural steels and materials such as aluminum and copper of higher purity. Being able to control the grain size in the material allows customization of several aspects of the material behavior. Important properties such as strength, ductility, fatigue life as well as wear and corrosion resistance depend on the microstructure grain size. The presence of impurities and added particles in the material will influence the recrystallization kinetics and the final grain size

both due to retardation of migrating grain boundaries through Zener pinning, cf. eq. (8), and due to particle stimulated nucleation. Considering relatively small particles of diameter less than 1 μm, the dominating mechanism will be Zener pinning [71, 4].

Fig. 7 shows how the simulated recrystallization process is retarded in the presence of impurity particles at the temperatures $T = 725$ K and $T = 775$ K. It is clearly seen from Fig. 7 how smaller particles more efficiently retards recrystallization compared to larger particles, in agreement with eq. (8). To obtain the plots in Fig. 7, the original Zener parameters $z_i = [3/2, 1]$ were used. Recalling eq. (8), it can be noted that the so-called particle dispersion level, i.e. the ratio $f_\mathrm{v}/r_\mathrm{p}$, enters as an important parameter. This quantity is a characteristic descriptor of the influence of impurities on the recrystallization behavior. Following [4], the recrystallization process is different within different ranges of $f_\mathrm{v}/r_\mathrm{p}$. For low values of $f_\mathrm{v}/r_\mathrm{p}$, the final average grain size is limited by grain growth, i.e. by the availability of nucleation sites in the microstructure. For some intermediate values of $f_\mathrm{v}/r_\mathrm{p}$, a minimum grain size is obtained during processing at elevated temperatures. This may not be a distinct minimum due to heterogeneous particle distribution and local variations. Instead, the minimum recrystallized grain size can be observed over an interval of particle dispersion levels. The grain evolution in this transition regime where the driving pressure is balanced by the particle drag pressure, acting on the grain boundaries, is referred to as "percolation recrystallization" in [19]. Finally, for larger values of $f_\mathrm{v}/r_\mathrm{p}$, the influence of Zener pinning is such that recrystallization is increasingly restricted until the point where recrystallization no longer occurs. The values of $f_\mathrm{v}/r_\mathrm{p}$ which minimize the final grain size then appears as important input in the design of customized fine-grained materials. Regarding the particle dispersion level $f_\mathrm{v}/r_\mathrm{p}$, it can be noted that this measure should be used with caution if the parameter $z_2 \neq 1$, cf. eq. (8).

Fig. 8 shows how the final grain size at different temperatures varies with the particle dispersion level. The particle size is kept constant at $r_\mathrm{p} = 0.1$ μm while the volume fraction f_v is varied. The final grain sizes on the vertical axes are normalized by the final grain size at each temperature, obtained for the pure copper material, i.e. with $f_\mathrm{v} = 0$. The symbols in the plots in Fig. 8 show simulation results for different values of the particle dispersion level and the solid lines are cubic splines, drawn through the data points just in order to indicate the trends in the data. The plots in Fig. 8 are obtained using the original parameter set $z_i = [3/2, 1]$. The existence of an optimum particle dispersion level $f_\mathrm{v}/r_\mathrm{p}$ that minimizes the final grain size, as discussed previously, is evident in Fig. 8 where the final grain size reaches a minimum at each of the temperatures. This minimum is, however, found over an interval of particle dispersion levels at some of the temperatures. This is especially true for the lower temperatures of $T = 725$ K and $T = 775$ K in Figs. 8a and 8b. As the temperature is increased, these minima tend to occur for smaller values of the particle dispersion level, i.e. for larger particles if f_v is kept constant or alternatively for smaller particle volume fractions if r_p is kept constant. Noting the temperature dependence of the grain boundary mobility parameter m_0 in Table 2, it is seen that the mobility is lowered as the temperature is increased. Since the grain boundary velocity is given by $v = mp$ according to eq. (6), the progression of recrystallization will be more efficiently retarded by Zener pinning, i.e. by lower magnitudes of the driving pressure p, as the temperature is increased. This explains the shift of the minima in the plots in Fig. 8 towards lower values of $f_\mathrm{v}/r_\mathrm{p}$ as increased temperatures are considered.

The minimum values of the final, normalized, grain sizes are shown in Table 4 along with the approximate values of the particle dispersion level at which the minimum values occur. Table 4 shows the normalized final grain size, as in Fig. 8, i.e. the final grain size is normalized using the final grain size in the absence of impurity particles. The grain size values in Table 4 thus show the

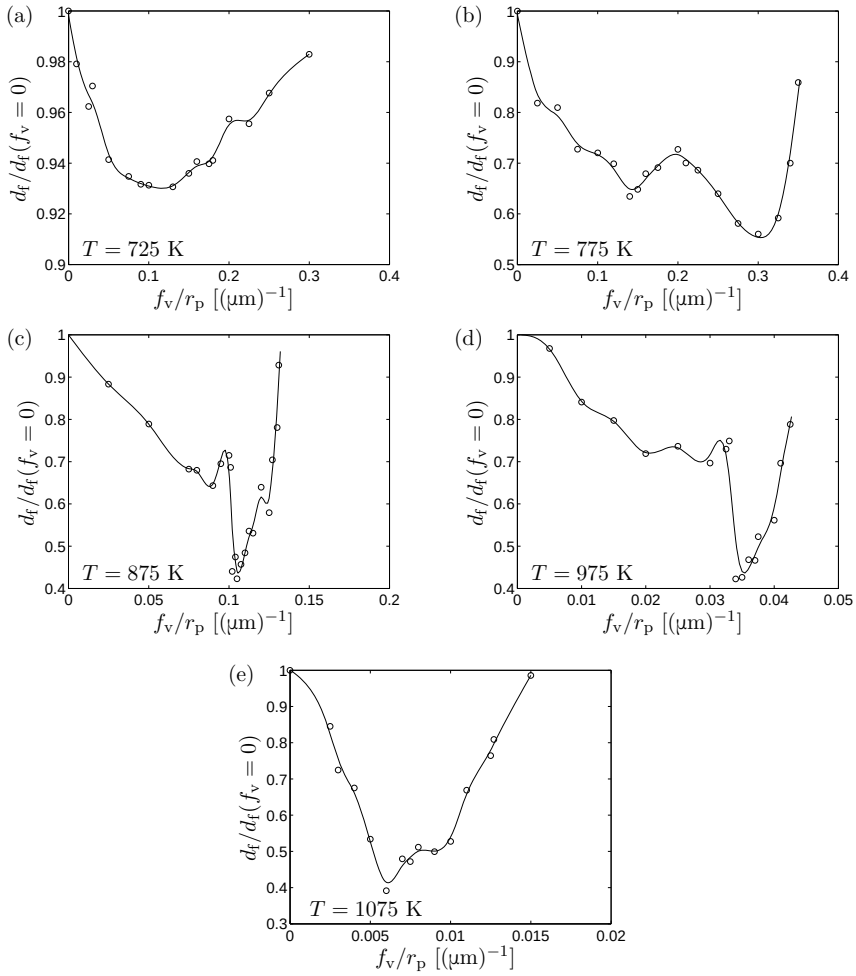

Figure 8: Influence on recrystallization from a homogeneous distribution of small impurity particles. Final grain size (normalized) after recrystallization as function of the particle dispersion level f_v/r_p for a fixed particle size of $r_p = 0.1$ μm. Results are shown at different temperatures. The circles show the actual simulation results while the solid lines are cubic spline interpolations, included simply to indicate the trends in the results. Note that the intervals on the axes differ between the figures.

Table 4: Approximate particle dispersion levels $f_\mathrm{v}/r_\mathrm{p}$ resulting in minimum final, normalized, grain size at different temperatures, cf. Fig. 8. Note that the values are indicative rather than absolute.

T [K]	$f_\mathrm{v}/r_\mathrm{p}$ $[(\mu\mathrm{m})^{-1}]$	$d_\mathrm{f}/d_\mathrm{f}(f_\mathrm{v}=0)$
725	0.12	0.95
775	0.3	0.55
875	0.11	0.45
975	0.035	0.45
1075	0.006	0.4

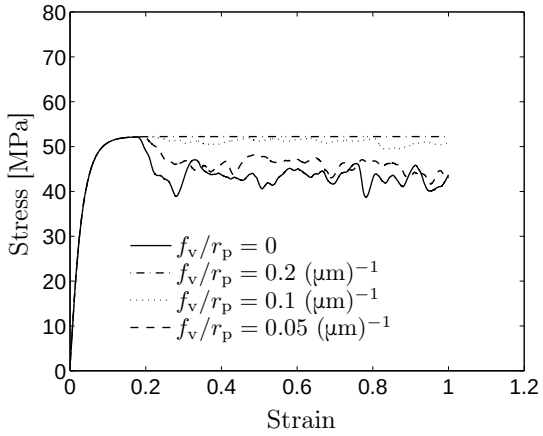

Figure 9: Effects on the flow stress at $T = 875$ K from increasing the particle dispersion level $f_\mathrm{v}/r_\mathrm{p}$, with $r_\mathrm{p} = 0.1$ μm. Also cf. Fig. 8c.

relative reduction in final grain size that can be obtained for the particle dispersion levels stated at each temperature. It can be noted that the final grain size can be reduced by approximately 50-60 % if controlled amounts of particles are added to the initially pure copper material.

Fig. 9 shows how the simulated flow stress behavior at $T = 875$ K is influenced by different values of the particle dispersion level $f_\mathrm{v}/r_\mathrm{p}$. Comparing Fig. 8c with Fig. 9, it can be noted that as the particle dispersion level approaches a value of approximately 0.1, the flow stress behavior is more or less unaffected by the recrystallization. The initial flow stress peak and the subsequent oscillations are replaced by a flow stress that saturates at a constant level as predicted by the material hardening, i.e. the dislocation density evolution law in eq. (1). The vanishing flow stress oscillations correspond to the final grain size reaching its minimum value, as seen in Fig. 8c.

If the original set of Zener parameters $z_i = [3/2, 1]$ are replaced by the modified set $z_i = [0.33, 0.87]$, the approximation of rigid grain boundaries in the original Zener formulation is relaxed [42, 43, 44]. This modification accounts for the tendency of the grain boundaries to bow out between pinning particles. Since the parameter values, and most predominantly so the value of z_1, are lower in the modified set, the retarding pressure on the boundaries due to particles will be less than in the original parameter set by Zener [41]. This will result in the recrystallization kinetics being less retarded by the modified parameter set $z_i = [0.33, 0.87]$ as compared to the original values $z_i = [3/2, 1]$. This is evident from Fig. 10 where the recrystallized volume fraction is shown as a function of time for $f_\mathrm{v} = 0.05$ and $r_\mathrm{p} = 0.2$ μm. The plots show the behavior at different temperatures in the absence of particles, i.e. $z_1 = 0$, with the original parameter set $z_i = [3/2, 1]$

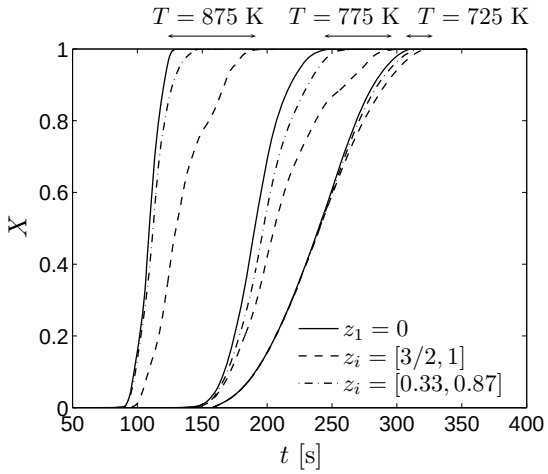

Figure 10: Effect of particle drag on the recrystallization kinetics using the modified Zener parameters $z_i = [0.33, 0.87]$ (dashed lines) compared to the original parameter set $z_i = [3/2, 1]$ (dash-dotted lines). For comparison also the behavior in the absence of particles is included (solid lines). The results are shown at different temperatures with $f_\mathrm{v} = 0.05$ and $r_\mathrm{p} = 0.2$ μm.

and with the modified set $z_i = [0.33, 0.87]$.

5 Concluding remarks

A micromechanical model for dynamic recrystallization, including particle drag, is established. The model is employed in a 3D cellular automaton algorithm with model parameters pertaining to pure copper. This allows studies of the microstructure evolution in a representative volume element exposed to deformation at elevated temperatures to be performed. In addition, homogenization of the dislocation density in the representative volume element also makes macroscopic properties, such as the flow stress behavior, available. The macroscopic flow stress obtained from the simulations correspond well to experimental data taken from the literature. As increased temperatures are considered, the expected transition from single/peak, relatively stable flow, into serrated multiple-peak flow is captured in the simulations. The microstructure evolution in terms of average grain size is also in agreement with experiments. In addition, the influence of changed initial average grain size is studied. In accordance with experimental data, a reduced initial grain size results in increasingly oscillatory flow stress behavior whereas an increased initial grain size stabilizes it.

To further verify the simulation results, comparisons are made with classical Kolmogorov-/Johnson/Mehl/Avrami (KJMA) theory. The expected change in the value of the Avrami exponent is found as conditions resembling site/saturated nucleation at lower temperatures gradually changes into conditions of continuous nucleation at higher temperatures. Introducing impurity particles into the material influences the recrystallization kinetics by reducing, or even pinning, mobile grain boundaries. The changed recrystallization kinetics at different temperatures and using different particle sizes are studied. As expected, the progression of recrystallization is retarded by the presence of impurities and this effect is more pronounced as smaller particles are considered.

Control of the grain size using deliberately added particles is an important industrial application, allowing tailoring of material properties. By changing the particle dispersion level, i.e. the

volume fraction of particles and/or the typical particle size, optimum processing conditions can be identified. For certain intervals of the particle dispersion level, the final grain size can be reduced by 50-60 %, depending on processing temperature.

The proposed model provides a versatile tool for analysis of microstructure evolution and related control of material properties. By use of a cellular automaton formulation, excellent computational efficiency together with high spatial and temporal resolution of the microstructure changes is obtained.

Acknowledgement

H. Hallberg gratefully acknowledges funding from the Swedish Research Council under grant C0423101.

References

[1] T. Sakai and J.J. Jonas. Dynamic recrystallization: Mechanical and microstructural considerations. *Acta Metall. Mater.*, 32(2):189–209, 1984.
[2] T. Sakai. Dynamic recrystallization microstructures under hot working conditions. *J. Mater. Process. Technol.*, 53:349–361, 1995.
[3] W. Gao, A. Belyakov, H. Miura, and T. Sakai. Dynamic recrystallization of copper polycrystals with different purities. *Mater. Sci. Eng.*, A265:233–239, 1999.
[4] F.J. Humphreys and M. Hatherly. *Recrystallization and related annealing phenomena*. Pergamon, New York, second edition, 2004.
[5] F.J. Humphreys. A unified theory of recovery, recrystallization and grain growth, based on stability and growth of cellular microstructures - I. The basic model. *Acta Mater.*, 45(10):4231–4240, 1997.
[6] F.J. Humphreys. A unified theory of recovery, recrystallization and grain growth, based on stability and growth of cellular microstructures - I. The effect of second-phase particles. *Acta Mater.*, 45(12):5031–5039, 1997.
[7] M.P. Anderson, D.J. Srolovitz, G.S. Grest, and P.S. Sahni. Computer simulation of grain growth – I. Kinetics. *Acta Metall. Mater.*, 32:783–791, 1984.
[8] D.J. Srolovitz, G.S. Grest, and M.P. Anderson. Computer simulation of recrystallization - I. Homogeneous nucleation and growth. *Acta Metall. Mater.*, 34:1833–1845, 1986.
[9] D.J. Srolovitz, G.S. Grest, M.P. Anderson, and Rollett. Computer simulation of recrystallization - II. Heterogeneous nucleation and growth. *Acta Metall. Mater.*, 36:2115–2128, 1988.
[10] A.D. Rollett, D.J. Srolovitz, M.P. Anderson, and R.D. Doherty. Computer simulation of recrystallization - III. Influence of a dispersion of fine particles. *Acta Metall. Mater.*, 40:3475–3495, 1992.
[11] P. Peczak and M.J. Luton. A Monte Carlo study of influence of dynamic recovery on dynamic recrystallization. *Acta Metall. Mater.*, 41(1):59–71, 1993.
[12] C.H.J. Davies. The effect of neighbourhood on the kinetics of a cellular automaton recrystallization model. *Scripta Metall. Mater.*, 33(7):1139–1143, 1995.
[13] D. Raabe. Cellular automata in materials science with particular reference to recrystallization simulation. *Annu. Rev. Mater. Res.*, 32:53–76, 2002.
[14] H.W. Hesselbarth and I.R. Göbel. Simulation of recrystallization by cellular automata. *Acta Metall. Mater.*, 39(9):2135–2143, 1991.
[15] R.L. Goetz and V. Seetharaman. Modeling of dynamic recrystallization using cellular automata. *Scripta Metall. Mater.*, 38(3):405–413, 1998.
[16] R. Ding and Z.X. Guo. Coupled quantitative simulation of microstructural evolution and plastic flow during dynamic recrystallization. *Acta Mater.*, 49:3163–3175, 2001.
[17] G. Kugler and R. Turk. Modeling the dynamic recrystallization under multi-stage hot deformation. *Acta Mater.*, 52:4659–4668, 2004.
[18] N. Yazdipour, C.H.J. Davies, and P.D. Hodgson. Microstructural modeling of dynamic recrystallization using irregular cellular automata. *Comp. Mater. Sci.*, 44:566–576, 2008.
[19] D. Raabe and L. Hantcherli. 2D cellular automaton simulation of the recrystallization texture of an IF sheet steel under consideration of Zener pinning. *Comp. Mater. Sci.*, 34:299–313, 2005.
[20] P. Mukhopadhyay, M. Loeck, and G. Gottstein. A cellular operator model for the simulation of static recrystallization. *Acta Mater.*, 55:551–564, 2007.
[21] D. Raabe. Introduction of a scalable three-dimensional cellular automaton with probabilistic switching rule for the discrete mesoscale simulation of recrystallization phenomena. *Phil. Mag. A*, 79:2339–2358, 1999.
[22] A.D. Rollett and D. Raabe. A hybrid model for mesoscopic simulation of recrystallization. *Comp. Mater. Sci.*, 21:69–78, 2001.
[23] A.M. Wusatowska-Sarnek, H. Miura, and T. Sakai. Nucleation and microtexture development under dynamic recrystallization of copper. *Mater. Sci. Eng.*, A323:177–186, 2002.
[24] F. Lefevre-Schlick, Y. Brechet, H.S. Zurob, G. Purdy, and D. Embury. On the activation of recrystallization nucleation sites in Cu and Fe. *Mater. Sci. Eng.*, A502:70–78, 2009.
[25] H. Hallberg, M. Wallin, and M. Ristinmaa. Modeling of discontinuous dynamic recrystallization in pure Cu using a probabilistic cellular automaton. *Comp. Mater. Sci.*, 49(1):25–34, 2010.
[26] Y. Estrin and H. Mecking. A unified phenomenological description of work hardening and creep based on one-parameter models. *Acta Metall. Mater.*, 32(1):57–70, 1984.
[27] H. Mecking, B. Nicklas, N. Zarubova, and U.F. Kocks. A "universal" temperature scale for plastic flow. *Acta Metall. Mater.*, 34(3):527–535, 1986.
[28] U.F. Kocks and H. Mecking. Physics and phenomenology of strain hardening: the FCC case. *Prog. Mater. Sci.*, 48:171–273, 2003.

[29] A.S. Krausz and K. Krausz, editors. *Unified Constitutive Laws of Plastic Deformation*, chapter 2, pages 69–106. Academic Press, 1996.
[30] L.M. Cheng, W.J. Poole, J.D. Embury, and D.J. Lloyd. The influence of precipitation on the work-hardening behavior of the Aluminum alloys AA6111 and AA7030. *Metall. Mater. Trans.*, 34A:247–2481, 2003.
[31] H. Hallberg and M. Ristinmaa. Microstructure evolution influenced by dislocation density gradients modeled in a reaction-diffusion system. *Comp. Mater. Sci.*, 67:373–383, 2013.
[32] P. Peczak and M.J. Luton. The effect of nucleation models on dynamic recrystallization. I. Homogeneous stored energy distribution. *Phil. Mag. B*, 68(1):115–144, 1993.
[33] P. Peczak and M. J. Luton. The effect of nucleation models on dynamic recrystallization. II. Heterogeneous stored-energy distribution. *Phil. Mag. B*, 70(4):817–849, 1993.
[34] P. Peczak. A Monte Carlo study of influence of deformation temperature on dynamic recrystallization. *Acta Metall. Mater.*, 43(3):1279–1291, 1995.
[35] C. Zheng, N. Xiao, D. Li, and Y. Li. Mesoscopic modeling of austenite static recrystallization in a low carbon steel using a coupled simulation method. *Comp. Mater. Sci.*, 45:568–575, 2009.
[36] D.G. Cram, X.Y. Fang, H.S. Zurob, Y.J.M. Bréchet, and C.R. Hutchinson. The effect of solute on discontinuous dynamic recrystallization. *Acta Mater.*, 60:6390–6404, 2012.
[37] J.E. Bailey and P.B. Hirsch. The recrystallization process in some polycrystalline metals. *Proc. R. Soc., London A*, 267(1328):11–30, 1962.
[38] W. Roberts and B. Ahlbom. A nucleation criterion for dynamic recrystallization during hot working. *Acta Metall. Mater.*, 26:801–813, 1978.
[39] J. E. Burke and D. Turnbull. Recrystallization and grain growth. *Prog. Met. Phys.*, 3:220–292, 1952.
[40] N. Ravichandran and Y.V.R.K. Prasad. Influence of oxygen on dynamic recrystallization during hot working of polycrystalline copper. *Mater. Sci. Eng.*, A156:195–204, 1992.
[41] C.S. Smith. Grains, Phases and Interfaces: An Interpretation of Microstructure. *Trans. Am. Inst. Min. Met. Eng.*, 175:15–51, 1948.
[42] N. Louat. The resistance to normal grain growth from a dispersion of spherical particles. *Acta Metall. Mater.*, 30:1291–1294, 1982.
[43] E. Nes, N. Ryum, and O. Hunderi. On the Zener drag. *Acta Metall. Mater.*, 33(1):11–22, 1985.
[44] O. Hunderi, E. Nes, and N. Ryum. On the Zener drag – Addendum. *Acta Metall. Mater.*, 37(1):129–133, 1989.
[45] P.A. Manohar, M. Ferry, and T. Chandra. Five decades of the Zener equation. *Iron and Steel Institute of Japan*, 38:913–924, 1998.
[46] D. Wolf. A Read-Shockley model for high-angle grain boundaries. *Scripta Metall. Mater.*, 23:1713–1718, 1989.
[47] H.-J. Bunge. *Texture analysis in materials science*. Cuvillier Verlag Göttingen, 1993.
[48] G. Zhu, W. Mao, and Y. Yu. Calculation of misorientation distribution between recrystallized grains and deformed matrix. *Scripta Materialia*, 42:37–41, 2000.
[49] M. G. Glavicic, P. A. Kobryn, T. R. Bieler, and S. L. Semiatin. A method to determine the orientation of the high-temperature beta phase from measured EBSD data for the low-temperature alpha phase in Ti-6Al-4V. *Materials Science and Engineering A*, 346:50–59, 2003.
[50] N. L. Vasiliev, S. V. Shevchenko, and S. L. Semiatin. Effect of the boundaries of crystalline grains of a special geometry on the kinetics of recrystallization and growth of grains. *Ukranian Journal of Physics*, 53(1):27–35, 2008.
[51] F. Montheillet, O. Lurdos, and G. Damamme. A grain scale approach for modeling steady-state discontinuous dynamic recrystallization. *Acta Mater.*, 57:1602–1612, 2009.
[52] R.E. Smallman and R.J. Bishop. *Modern Physical Metallurgy and Materials Engineering*. Butterworth-Heinemann, sixth edition, 1999.
[53] L. Blaz, T. Sakai, and J.J. Jonas. Effect of initial grain-size on dynamic recrystallization of copper. *Met. Sci.*, 17(12):609–616, 1983.
[54] J. Gruber, H.M. Miller, T.D. Hoffmann, G.S. Rohrer, and A.D. Rollett. Misorientation texture development during grain growth. Part I: Simulation and experiment. *Acta Mater.*, 57:6102–6112, 2009.
[55] K. Kremeyer. Cellular automata investigations of binary solidifications. *J. Comput. Phys.*, 142:243–262, 1998.
[56] Y.J. Lan, D.Z. Li, and Y.Y. Li. A mesoscale cellular automaton model for curvature-driven grain growth. *Metall. Mater. Trans.*, 37B:119–129, 2006.
[57] H.S. Zurob, Y. Brechet, and J. Dunlop. Quantitative crietrion for recrystallization nucleation in single-phase alloys: Prediction of critical strains and incubation times. *Acta Mater.*, 54:3983–3990, 2006.
[58] D.G. Cram, H.S. Zurob, Y.J.M. Bréchet, and C.R. Hutchinson. Modelling discontinuous dynamic recrystallization using a physically based model for nucleation. *Acta Mater.*, 57:5218–5228, 2009.
[59] N. A. Gjostein and F. N. Rhines. Absolute interfacial energies of [001] tilt and twist grain boundaries in copper. *Acta Metall. Mater.*, 7:319–330, May 1959.
[60] R. Viswanathan and C. Bauer. Kinetics of grain boundary migration in copper bicrystals with [001] rotation axes. *Acta Metall. Mater.*, 21(8):1099–1109, 1973.
[61] H.S. Kim, Y. Estrin, E.Y. Gutmanas, and C.K. Rhee. A constitutive model for densification of metal compacts: the case of copper. *Mater. Sci. Eng.*, 307:67–73, 2001.
[62] H. Mecking and U.F. Kocks. Kinetics of flow and strain-hardening. *Acta Metall. Mater.*, 29:1865–1875, 1981.
[63] H.J. Frost and M.F. Ashby. *Deformation-Mechanism Maps*. Pergamon Press, 1982.
[64] O. Bouaziz and P. Buessler. Iso-work increment assumption for heterogeneous material behavior modelling. *Adv. Eng. Mat.*, 6(1-2):79–83, 2004.
[65] M. Avrami. Kinetics of phase change, I. general theory. *J. Chem. Phys.*, 7:1103–1112, 1939.
[66] M. Avrami. Kinetics of phase change, II. Transformation-time relations for random distribution of nuclei. *J. Chem. Phys.*, 8:212–224, 1940.
[67] M. Avrami. Kinetics of phase change, III. Granulation, phase change and microstructure. *J. Chem. Phys.*, 9:177–184, 1941.
[68] P. Karduck, G. Gottstein, and H. Mecking. Deformation structure and nucleation of dynamic recrystallization in copper single crystals. *Acta Metall. Mater.*, 31(10):1525–1536, 1983.
[69] T. Furu, K. Marthinsen, and E. Nes. Modelling recrystallization. *Mater Sci Tech*, 6:1093–1102, 1990.
[70] M.T. Todinov. On some limitations of the Johnson-Mehl-Avrami-Kolmogorov equation. *Acta Mater*, 48:4217–4224, 2000.
[71] F.J. Humphreys and M.G. Ardakani. Grain boundary migration and Zener pinning in particle-containing copper crystals. *Acta Materialia*, 44(7):2717–2727, 1996.